Highly efficient excitation of LP_{01} mode in ring-core fibers by tapering for optimizing OAM generation

Chunxiang Zhang (张春香), Fufei Pang (庞拂飞), Huanhuan Liu (刘奂奂), Lifei Chen (陈丽飞), Junfeng Yang (杨俊锋), Jianxiang Wen (文建湘), and Tingyun Wang (王廷云)*

Key Laboratory of Specialty Fiber Optics and Optical Access Networks, Joint International Research Laboratory of Specialty Fiber Optics and Advanced Communication, Shanghai Institute for Advanced Communication and Data Science, Shanghai University, Shanghai 200444, China

**Corresponding author: tywang@shu.edu.cn*

Received September 2, 2019; accepted November 7, 2019; posted online January 2, 2020

We have demonstrated the highly efficient excitation of the linearly polarized mode (LP_{01}) in ring-core fibers (RCFs) by tapering the spliced point between the RCF and the standard single-mode fiber (SMF) to optimize all-fiber orbital angular momentum (OAM) generation. The tapering technique has been investigated theoretically and experimentally. Before tapering, only 50% of light can be coupled from SMFs to RCFs. The modal interference spectrum with an extinction ratio (ER) of ~9 dB is observed, showing that higher-order modes are excited in RCF. By tapering the spliced point, 90% of light is coupled, and the ER is minimized to be ~2 dB, indicating that the higher-order modes are effectively suppressed by tapering. Such tapered spliced points of RCF–SMF are further applied for all-fiber OAM generation. The efficiencies of OAM_{+1} and OAM_{-1} generation are found to be enhanced by approximately 11.66% and 12.41%, respectively, showing that the tapered spliced point of the RCF–SMF is a feasible way to optimize OAM generation.

Keywords: ring-core fiber; single-mode fiber; all-fiber orbital angular momentum generation; tapering technology.

doi: 10.3788/COL202018.020602.

Nowadays, vortex beams, carrying orbital angular momentum (OAM), have been known as the hot spots and shown great potential in various fields such as optical micro-manipulation[1], optical sensors[2], optical transmission[3,4], optical lasers[5], and amplifiers[6,7]. OAM has its own unique helical phase characteristic. The count of modes in the vortex beam can be infinite, and the mode is orthogonal to each other[8,9]. The generation of OAM with high purity and high stability, especially, the first-order OAM in fiber, has attracted much attention. The first-order OAM modes can be composed of the linearly polarized modes (LP_{11}^{x} and LP_{11}^{y} mode) with phase difference of $\pi/2$, which is generally excited by the LP_{01} mode[10]. Therefore, to ensure the high excitation efficiency of the LP_{11} mode, the purity of the LP_{01} mode must be high. To obtain stable OAM, many vortex fibers have been explored, including the triple-cladding fiber[11], photonic crystal fiber[12], helical-core fiber[13], etc. Different from the above vortex fibers, the ring-core fiber (RCF) with the ring-shaped refractive index, which is similar to the pattern of the vortex beam, is superior. On one hand, the RCF has a large cut-off propagation constant of the mode area, and the LP_{01} mode in the RCF has non-zero cut-off frequency. The lower-order modes in RCF have a larger propagation constant and can occupy more energy. On the other hand, RCF can achieve a large mode efficient index difference, which enables it to avoid the strong mode coupling between azimuthal higher-order modes[14].

In traditional OAM mode generation techniques, free-space optical components are used to couple the OAM beam into RCFs[15]. But, it needs highly accurate alignment and exhibits relatively high coupling loss. An alternative solution is to use an all-fiber OAM generation system. Previous reports have shown few-mode fibers (FMFs) spliced with a standard single-mode fiber (SMF) for OAM generation[16,17]. The LP_{01} mode of the SMF can effectively excite the LP_{01} mode of the FMF because both fibers have a similar structure. As the RCF shows greater merits of OAM transmission than common FMFs, it is expected to achieve all-fiber excitation of the desired modes with RCFs[18,19]. However, due to the unique structure of the RCF, the splicing of the RCF and the SMF will cause loss, and thus all-fiber OAM generation in RCF faces a challenge. So, it is necessary to reduce the loss between the SMF and the RCF. Further, highly efficient excitation of the LP_{01} mode can be applied in mode division multiplexed (MDM) transmission[20], temperature sensors[21], and fiber lasers[22].

Fiber tapering technology can be used to improve the coupling efficiency between two different types of fiber, such as by tapering the spliced point between the SMF and multimode fiber[23], dual-core fiber[24], hollow-core fiber[25], and helical-core fiber[26]. In this paper, we have proposed and investigated an efficient method to excite the LP_{01} mode of the RCF by tapering the spliced point between the RCF and the SMF, which can optimize the efficiency of the OAM generation system with RCFs. Simulations accurately predict the optimal radius of the tapered fiber and guide the experiment on tapering the spliced point. The simulation results show that the coupling efficiency of different modes in the RCF can be optimized by changing the tapering radius. The coupling efficiency of 92% can be theoretically achieved when the waist radius is approximately 5 μm. Through tapering, the extinction ratio (ER) shown in the interference spectrum obviously reduces, and the transmission increases. The experiment on the improvement of OAM generation is conducted to verify high excitation of the LP_{01} mode in the RCF.

The schematic diagram of the fiber structure as well as the refractive index profile for the SMF and RCF is shown in Figs. 1(a) and 1(b), respectively. Figure 1(c) represents an ideal taper for exciting the LP_{01} mode in the RCF. The SMF and RCF, which have the same outer-cladding diameter, can be spliced together directly. However, because of the different structure, the exciting efficiency of the LP_{01} mode in the ring core is limited with higher-order modes excitation. By applying tapering technology to the spliced point between these two fibers, the exciting efficiency of the LP_{01} mode in the RCF is expected to be evidently improved.

The tapered region consists of three parts: the upper transition zone, the taper waist, and the lower transition zone. In the lower transition zone, the fundamental core mode LP_{01} converts from the SMF core to the tapered-cladding waveguide. In general, the taper structure will cause the energy loss because of the non-adiabatic taper structure[27]. However, in this work, the taper structure is used as a mode field adaptor to improve the coupling efficiency between two different types of fiber. When the radius of the waist is smaller, the mode fields in the two different types of fiber are more similar, and thus a high coupling efficiency of the LP_{01} mode can be obtained. If we aim to excite the fundamental core mode LP_{01} of the RCF through the tapering structure efficiently, the adiabatic condition must be satisfied. It requires the taper angle θ of the transition zone to be small enough as in the following:

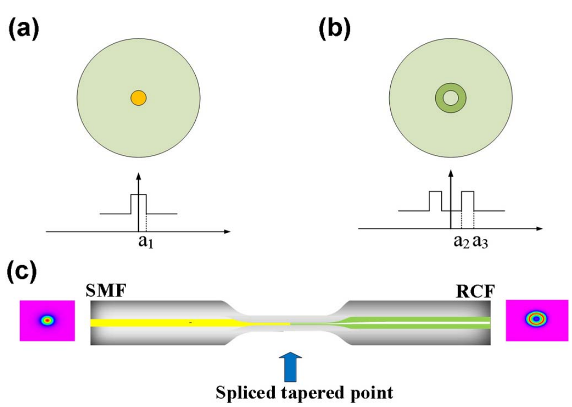

Fig. 1. Schematic diagram of fiber structure and refractive index profile for (a) single-mode fiber (SMF) and (b) ring-core fiber (RCF); (c) schematic diagram of fusion splicing and tapering scheme for exciting the LP_{01} mode in the RCF with high efficiency.

$$\theta < \frac{\rho}{Z_t}, \tag{1}$$

where Z_t is the locally tapered fiber length, and ρ is the diameter of the tapered fiber. The small taper angle θ can ensure avoiding the mode coupling from the LP_{01} mode to the LP_{02} mode and other higher-order modes. Furthermore, at the lower transition zone, the small taper angle can also ensure adiabatic coupling from the LP_{01} mode of the taper waist to the LP_{01} mode of the RCF. For the SMF–RCF taper, the coupling efficiency (η) for calculating the overlap integral between modes in the SMF and modes in the RCF can be described as follows:

$$\eta = \frac{\iint E_a E_b{}^* \mathrm{d}x\mathrm{d}y}{\sqrt{\left|\iint E_a E_a{}^* \mathrm{d}x\mathrm{d}y\right| \cdot \left|\iint E_b E_b{}^* \mathrm{d}x\mathrm{d}y\right|}}, \tag{2}$$

where E_a and E_b are the electric field of mode in the taper waist of the SMF and the RCF, respectively.

In order to optimize parameters of the SMF–RCF taper, simulations on the tapered fiber for the excitation of the LP_{01} mode in RCF are investigated. The RCF used in our discussion is designed and fabricated by our laboratory, and the structure of the RCF is shown in Fig. 1(b). The radius of the inner cladding is 4 μm, and the thickness of the high-index core is 8 μm. The relative refractive index difference between inner cladding and high-index core is 0.0272. The radius of the outer cladding of the RCF is consistent with that of the SMF (SMF-28). During tapering of the spliced point, the fiber dimension changes following the law of conservation of volume[28]. The relationship between the radius of the tapered fiber (r) and stretch length (l) can be deduced as follows:

$$r(z) = \begin{cases} r_0\left\{-\frac{2\alpha[z+0.5(l+L_0)]}{(1-\alpha)L_0}\right\}^{-1/2\alpha}, & (z > z_0) \\ r_0\left(1+\frac{\alpha l}{L_0}\right)^{-1/2\alpha}, & (-z_0 < z < z_0) \\ r_0\left\{-\frac{2\alpha[-z+0.5(l+L_0)]}{(1-\alpha)L_0}\right\}^{-1/2\alpha}, & (z < -z_0) \end{cases} \tag{3}$$

where L_0 is the equivalent width of the initial flame, and α is a constant, which determines the relative rates of hot-zone change and taper elongation[29]. The range of α is from 0 to 1, and α determines the steep degree of the tapered fiber. The higher the rate of flame changes, the steeper the taper becomes. Here, $\alpha = 0.1$ and $L_0 = 2000$ μm are referred to in our simulated model by using a beam propagation method (BPM) under a commercial software (Rsoft).

As shown in Fig. 2, on the condition that two different stretched lengths are considered, it is an adiabatic taper for SMF because almost only the LP_{01} mode propagates in the taper waist of the SMF. The light blue curves show the change of energy in the taper cladding. The obvious difference between the SMF and the RCF in mode fields on the other side of the spliced point causes the large loss of the LP_{01} mode in the taper-cladding waveguide in

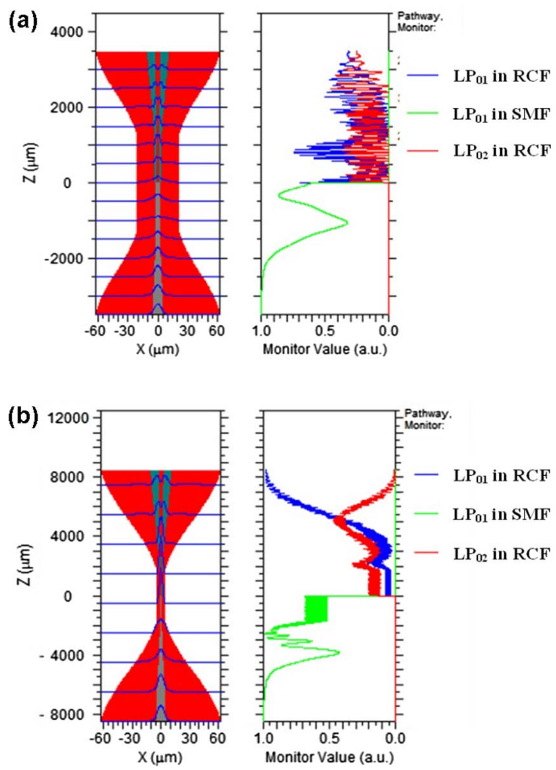

Fig. 2. Simulation of light propagation and coupling power evolution along the tapered fibers with different stretched lengths: (a) 5000 μm and (b) 16,000 μm.

Fig. 2(a). LP_{01} and LP_{02} modes can be monitored as the blue curve and green curve, which show great loss. In Fig. 2(b), mode field in the waist of the SMF matches well with that on the other side of the spliced point, and thus the light curve shows little change in the taper waist. The high coupling efficiency of the LP_{01} mode can be achieved under these conditions.

Because the stretched length has the decisive influence on the waist radius of the tapered fiber, the effect of stretched length on coupling efficiency is also investigated. Coupling efficiencies of LP_{01} and LP_{02} modes in RCF are computed with the stretched length ranging from 0 μm to 20,000 μm. According to Eq. (3), the waist radius is used to present the results more specifically and clearly. Figure 3 indicates the relationship between coupling efficiency and waist radius changing from 2 μm to 20 μm. When tapering the spliced point, propagation constants of modes excited decrease with the decreasing waist radius. In the certain waist radius, the LP_{02} mode propagates in the cladding, while the LP_{01} mode propagates in the high-index zone with the ring-shaped field distribution. The overlap integral between the LP_{01} mode in the SMF and the LP_{02} mode in the RCF gets larger. When the radius decreases to 12 μm, the LP_{01} mode begins propagating in the cladding. The overlap integral between the LP_{01} mode in the RCF and the LP_{01} mode in the SMF increases, so coupling efficiency of the LP_{01} mode shows an increasing trend. However, when the waist radius of the tapered fiber is smaller, the tapered fiber is fragile and hard to manufacture. The results indicate that the waist radius of 5 μm is the best choice for the tapered fiber. Coupling efficiency of the LP_{01} mode is up to 92%, as shown in Fig. 2(b), when the stretched length is 16,000 μm.

According to the calculated stretched length, the taper with a waist radius of 5.5 μm is applied in the experiment. The experimental setup of characterizing the SMF–RCF taper is given in Fig. 4. A super luminescent LED (SLED) used as a broadband light source can excite the LP_{01} mode of the SMF, and an optical spectrum analyzer (OSA, AQ6370C) is used to measure the transmission spectrum of the taper with and without the SMF pigtail, respectively. Without the SMF pigtail, the RCF is connected to the OSA directly, and all the guide modes can be detected. On the contrary, with splicing an SMF pigtail after the RCF, only the LP_{01} mode can be detected.

Figure 5 represents the measured transmission spectra of the SMF–RCF splicing point before and after tapering, respectively. Figure 5(a) reflects an increase in the total energy of the RCF after tapering, in which the black curve is the total energy before tapering the spliced point, and the red curve is the total energy after tapering the spliced point. Compared with the untapered fiber, tapering reduces the transmission loss by approximately 3 dB, indicating that more light can be coupled to the RCF. Compared with Fig. 5(a), Fig. 5(b) has an additional SMF between the output of the RCF and the input of the OSA. By including a piece of SMF, the mode interference spectrum can be monitored by using the OSA. Before tapering the spliced point, a periodic transmission

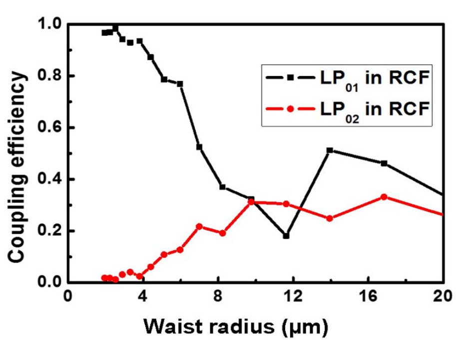

Fig. 3. Theoretical optimization of coupling efficiency in the relationship of waist radius.

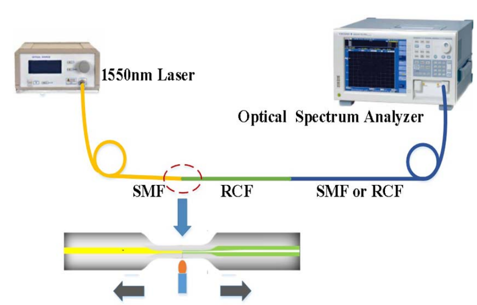

Fig. 4. Experimental setup of characterizing coupling efficiency and mode changes in the SMF–RCF taper.

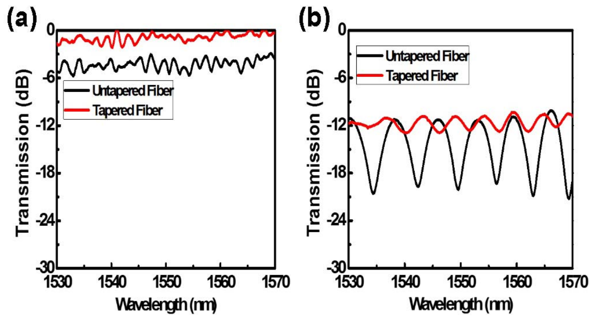

Fig. 5. Transmission of the SMF–RCF taper: (a) RCF connected to optical spectrum analyzer (OSA) directly; (b) RCF connected to the OSA with an SMF.

spectrum with a high ER of approximately 9 dB can be observed, which implies that mainly two modes are excited in the RCF. After tapering the SMF–RCF spliced point, an approximately 7 dB reduction in the ER is observed, which means that only the LP_{01} mode is excited and propagates in the RCF. Therefore, high-efficiency excitation of the LP_{01} mode in the RCF can be obtained by tapering. The polarization dependent loss is measured to be less than 0.2 dB, indicating a good polarization stability of the taper structure.

Further simulations to explain the transmission spectrum change resulting from the tapering are carried out. The modal coupling efficiency is computed from 1530 nm to 1570 nm. As it is shown in Fig. 6, approximately 50% light can be coupled to the LP_{01} and LP_{02} modes of the RCF theoretically before tapering. After tapering, obvious improvement in total power as well as the proportion of the LP_{01} mode is observed. It indicates that the LP_{02} mode of the RCF can be suppressed by tapering the spliced point theoretically; moreover, the SMF–RCF taper is a broadband optical component.

The developed SMF–RCF taper is further applied for first-order OAM mode generation. The pressure is applied on the RCF after the taper, as shown in Fig. 7(a). After pressing the RCF, higher modes constituting the OAM mode can be excited, and $\pi/2$ phase difference between LP_{11}^{x} and LP_{11}^{y} can be obtained because optical fiber

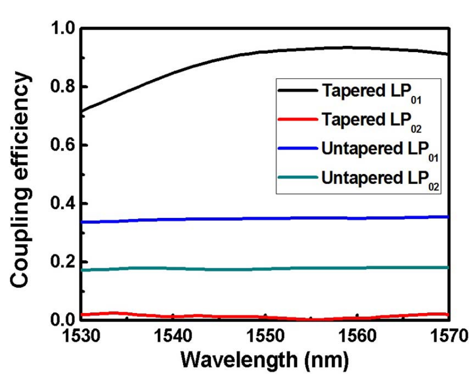

Fig. 6. The influence of wavelength on coupling efficiency of modes in the RCF from 1530 nm to 1570 nm.

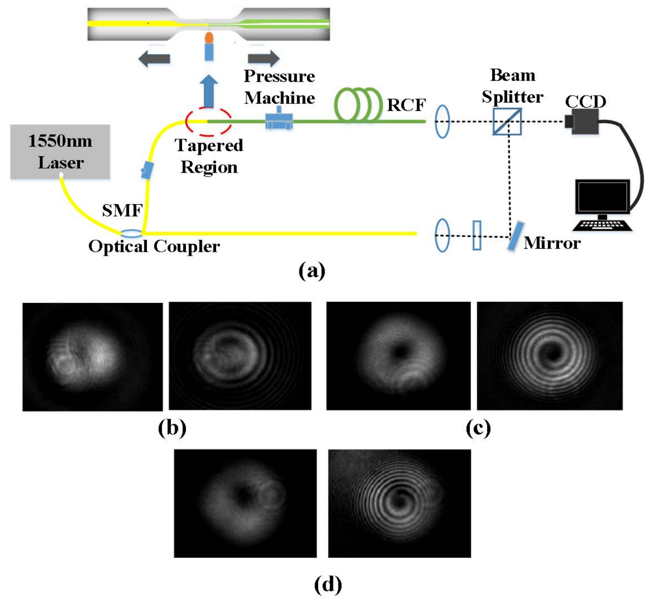

Fig. 7. (a) Experimental setup of orbital angular moment (OAM) generation and test system. (b) Mode field and interference fringe of the LP_{01} mode in the RCF. (c) Mode field and interference fringe of OAM_{+1}. (d) Mode field and interference fringe of OAM_{-1}.

symmetry is destroyed. In order to keep the broadband feature, a uniform pressure region of 5 cm is used instead of a mechanical long period grating. With increasing pressure, the LP_{01} mode of the RCF in Fig. 7(b) can be coupled to OAM_{+1}, as shown in the right of Fig. 7(c). After changing the polarization of the input light, OAM_{+1} can be converted to OAM_{-1}, as shown in Fig. 7(d). When the SMF is connected to the RCF directly, only 61.28% and 61.9% of light can be coupled to OAM_{+1} and OAM_{-1}, respectively, in the RCF. After tapering the spliced point, 72.94% and 74.31% of light can be coupled to OAM_{+1} and OAM_{-1}, respectively. Experimental result shows that tapering technology can improve coupling efficiency of OAM modes in the RCF.

In summary, we put forward an optimized method of OAM generation in an RCF by tapering the spliced point between the RCF and the SMF. The SMF–RCF taper, which can improve the coupling efficiency of the LP_{01} mode in the RCF, is researched. The overlap integral between the mode of the RCF and mode of the SMF is used to measure the coupling efficiency. To ensure that most of the light can be coupled to the RCF, the taper must be adiabatic for the SMF. The relationship of waist radius and the coupling efficiency is analyzed theoretically to obtain the optimal waist radius. When the waist radius is 5 μm, the coupling efficiency of modes in the RCF is improved up to 92%, and a 7 dB reduction in the ER can be obtained in the experiments. It is in accordance with the simulation results in the broadband characteristic. Further experiments on OAM generation by applying pressure on the RCF after the tapering are carried out. Compared to the OAM generation system without the

SMF-RCF taper, efficiencies of OAM_{+1} and OAM_{-1} generation are enhanced by approximately 11.66% and 12.41%, respectively, which indicates tapering technology can improve efficiency of mode coupling in an RCF. With the high excitation of the LP_{01} mode in RCFs by tapering the spliced point, further researches on all-fiber OAM generation in RCFs can be carried out.

This work was supported by the National Natural Science Foundation of China (Nos. 61635006, 61975108, and 61605108) and the Shuguang Program (No. 16SG35).

References

1. H. L. Zhou, J. J. Dong, S. Q. Yan, Y. F. Zhou, Y. F. Zhou, L. Shi, and X. L. Zhang, Opt. Express **22**, 17756 (2014).
2. R. D. Niederriter, M. E. Siemens, and J. T. Gopinath, in *Conference on Lasers and Electro-Optics* (2015), paper SM1L.5.
3. G. X. Zhu, Z. Y. Hu, X. Wu, C. Du, W. Y. Luo, Y. J. Chen, X. L. Cai, J. Liu, J. B. Zhu, and S. Y. Yu, Opt. Express **26**, 594 (2018).
4. X. Y. Fu, Y. W. Zhai, H. Zhou, J. Q. Zhang, C. Yin, and C. Q. Gao, Chin. Opt. Lett. **17**, 080602 (2019).
5. Z. M. Zhang, W. Wei, L. Q. Tang, J. Yang, J. W. Guo, L. Ding, and Y. G. Li, Chin. Opt. Lett. **16**, 110501 (2018).
6. J. X. Wen, X. Y. He, J. F. Xing, J. F. Yang, F. F. Pang, X. L. Zeng, Z. Y. Chen, and T. Y. Wang, IEEE Photon. J. **10**, 7105308 (2018).
7. J. F. Xing, J. X. Wen, J. Wang, F. F. Pang, Z. Y. Chen, Y. Q. Liu, and T. Y. Wang, Chin. Opt. Lett. **16**, 100604 (2018).
8. J. F. Ye, Y. Li, Y. H. Han, D. Deng, X. Y. Su, H. Song, J. M. Gao, and S. L. Qu, Opt. Lett. **42**, 3064 (2017).
9. J. F. Ye, Y. Li, Y. H. Han, D. Deng, Z. Y. Guo, J. M. Gao, Q. Q. Sun, Y. Liu, and S. L. Qu, Opt. Express **24**, 8310 (2016).
10. Y. Zhang, F. F. Pang, H. H. Liu, X. Q. Jin, S. J. Huang, Y. C. Li, J. X. Wen, Z. Y. Chen, M. Wang, and T. Y. Wang, IEEE Photon. J. **9**, 7101609 (2017).
11. N. Bozinovic, Y. Yue, Y. Ren, M. Tur, P. Kristensen, H. Huang, A. E. Willner, and S. Ramachandran, Science **340**, 1545 (2013).
12. H. Zhang, X. G. Zhang, H. Li, Y. F. Deng, L. X. Xi, X. F. Tang, and W. B. Zhang, Crystals **7**, 286 (2017).
13. N. Alexeyev, B. P. Lapin, and M. A. Yavorsky, Phys. Rev. A **78**, 13332 (2008).
14. L. B. Yuan, Z. H. Liu, and J. Yang, Opt. Lett. **31**, 3237 (2006).
15. J. F. Ye, Y. Li, Y. H. Han, D. Deng, X. Y. Su, H. Song, J. M. Gao, and S. L. Qu, Opt. Lett. **42**, 3064 (2017).
16. S. H. Li, Q. Mo, X. Hu, C. Du, and J. Wang, Opt. Lett. **40**, 4376 (2015).
17. S. Pidishety, S. Pachava, P. Gregg, S. Ramachandran, G. Brambilla, and B. Srinivasan, Opt. Lett. **42**, 4347 (2017).
18. P. Gregg, P. Kristensen, and S. Ramachandran, Optica **2**, 267 (2015).
19. C. Brunet, P. Vaity, Y. Messaddeq, S. LaRochelle, and L. A. Rusch, Opt. Express **22**, 26117 (2014).
20. T. Mori, T. Sakamoto, M. Wada, A. Urushibara, T. Yamamoto, and K. Nakajima, J. Lightwave Technol. **35**, 1936 (2017).
21. S. Chebaane, R. Ala, and M. Mohsen, in *International Conference on Advanced Systems and Electric Technologies* (2018), p. 17.
22. J. Liu, X. Liang, C. Sun, and S. Jian, Opt. Fiber Technol. **33**, 16 (2017).
23. Y. M. Jung, Y. C. Jeong, G. Brambilla, and D. J. Richardson, Opt. Lett. **34**, 2369 (2009).
24. Y. M. Jung, G. Brambilla, and D. J. Richardson, Opt. Express **16**, 14661 (2008).
25. S. Ravets, J. E. Hoffman, P. R. Kordell, J. D. Wong-Campos, S. L. Rolston, and L. A. Orozco, J. Opt. Soc. Am. A **30**, 2361 (2013).
26. H. Kim, J. K. Kim, Y. M. Jung, L. A. Vazquez-Zuniga, S. J. Lee, G. C. Choi, K. Oh, P. Wang, W. A. Clarkson, and Y. C. Jeong, Opt. Express **20**, 25562 (2012).
27. A. J. Fielding and C. C. Davis IEEE Photon. Technol. Lett. **14**, 53 (2002).
28. T. M. Zhou, Y. N. Zhang, B. Han, A. Z. Zhang, and D. X. Fu, Opt. Fiber Technol. **45**, 53 (2018).
29. T. A. Birks and Y. W. Li, J. Lightwave Technol. **10**, 432 (2002).